LQR based MIMO-PID controller for the vector control of an underdamped harmonic oscillator

Anis Kaci, Christophe Giraud-Audine, Frédéric Giraud, Michel Amberg, Betty Lemaire-Semail

LQR based MIMO-PID controller for the vector control of an underdamped harmonic oscillator

Anis Kaci*, Christophe Giraud-Audine, Frederic Giraud, Michel Amberg, Betty Lemaire-Semail

Univ. Lille, Arts et Metiers ParisTech, Centrale Lille, HEI, EA 2697 - L2EP – Laboratoire d'Electrotechnique et d'Electronique de Puissance, F-59000 Lille, France

Abstract

Modulated-Demodulated control (or vector control) allows to simultaneously impose amplitude and phase of a resonator. Moreover, the working frequency in the case of discrete-controller is substantially lower than the resonance frequency. However, the design of a such controller can be complex. In this paper, we outline a design directly in the baseband. To do so, the oscillator is modelled as a non-dimensional Multi-Input-Multi-Output system. An optimal control (Linear Quadratic Regulator) framework can then be used to design the controller. Thanks to ad-hoc performances criteria, the weighting matrices are systematically specified according to the desired closed-lop time response. The methodology is validated by an experimental results on a plate actuated using piezoelectric patches.

Keywords: Vector Control (demodulated-modulated control), Piezoelectric transducer, Linear Quadratic Regulator (LQR), Vibration control

1. Introduction

Many medical and industrial processes use resonating electromechanical systems e.g. in nebulizer, echography or ultrasonic welding. In some of these applications [1, 2], vibration need to be maintained at a given level of amplitude

*Corresponding author
Email address: anis.kaci@univ-lille.fr (Anis Kaci)

and track the resonance frequency in spite of the non-linearity and exogenous perturbations [3, 4].

Because these systems often operate at high frequencies, the implementation of a fast and precise closed-loop discrete-controller requires high sampling frequencies and fast computing capabilities. Therefore, some authors rather use open-loop control for which a perfect knowledge of the system is required. In MEMS, Borovic & al. [5] conclude that if the device has 2 positions, open-loop control is sufficient, but if the device has to be positioned between 0 and 100 %, then closed-loop control is preferred. For resonant devices, which operate at their resonance frequency, it is important to control the vibration amplitude, because the load can modify the damping or induce a non-linear behaviour [1]. Since this acoustic load is hardly predictable, closed-loop controls are implemented. Babitsky et al.[6] proposed a self-oscillating circuit to control the vibration at resonance without knowing the dynamic response of the system. In [7], a non-linear controller is designed in order to control the position of a Traveling Wave Ultrasonic Motor. The authors claim superior performances compared to a *Proportional-Integral* (PI) controller. However, dynamic responses was not studied.

As a consequence of the dramatic cost reduction of some electronic parts, like Digital Signal Processors (DSP) for instance, modulation-demodulation control structure becomes competitive [8]. This control consists in demodulating the measure by a sinusoidal signal in order to obtain the in-phase and in-quadrature components, and to modulate controller's outputs by the same signal. This method has shown good results for active damping of structures [9]. For Ultrasonic transducer, the method is called *Vector Control Method* as a reference to the control of Electromagnetic motors, and it has been successfully applied to the control of a Langevin transducer to be robust despite system's non linearities [10]. In this work, good dynamic results are obtained with PI controllers. The design of the controller is based on a simplified model assuming a weak coupling between the states, which allows to consider two *Single Input Single Output - Proportional Integral* (SISO-PI). However, this assumption limits the

closed-loop dynamics. In order to relax this limitation, this decoupling assumption must be dropped and a *Multi Input Multi Output* (MIMO) design is then necessary. However, the tuning of the controllers parameters are complicated as the system is MIMO [11]. In [12, 13, 14, 15, 16], the authors propose to use the *Linear Quadratic Regulator* (LQR) methodology to derive the SISO or MIMO-PID controllers. However, the choice of the Q and R matrices is still left to the designers judgement and experience, or using optimization procedure [15].

In this paper, the model of the oscillator in the baseband is reformulated to take into account the higher dynamics. A non-dimensional model is then derived for the sake of generality. Performances criteria describing the desired closed loop dynamic and the transient vibration envelop are then proposed. Based on these criteria, the weighting matrices coefficients can be directly expressed as a function of the desired closed-loop time response and thus the PID controller coefficients can be deduced.

The rest of the paper is organized as follows. In section 2, the normalized dynamic model of the resonant transducer in a demodulated form is presented. In section 3, the method to implement MIMO-PID controller based on the LQR design is recalled. The performances indexes are introduced, and their relation with the weighting matrices is studied, yielding a systematic procedure to design the controller. In the following part,the experimental set-up and protocol are explained. Experimental tests confirming the methodology are then presented. Finally, the paper ends with the conclusion in section 5.

2. Dynamic modelling

2.1. State space representation in the demodulated space

We consider a damped linear harmonic oscillator, which dynamic is given in a normalized form as follows:

$$\ddot{\eta}(t) + 2\xi\omega_n\dot{\eta}(t) + \omega_n^2\eta(t) = \omega_n^2 f(t) \tag{1}$$

Where $\eta(t)$ is the deflection of the resonator, ξ the damping factor, ω_n the resonance frequency, and $f(t)$ the external normalized force applied to the system which produces its oscillation. Actually, due to normalization $f(t)$ is rather the quasi-static displacement under the real load and it is expressed in meter (m). This model is actually general, and can represent for instance the dynamic of the behaviour of a given mode once projected in the modal basis either for a lumped parameters or a continuous system (see [17, p. 25] or [18, p.440] for instance). When the displacement η and the external force f are purely harmonic, one we can use their complex form as in the following equations:

$$\underline{\eta}(t) = (H_d(t) + jH_q(t))e^{j\omega t} \tag{2}$$

$$\underline{f}(t) = (F_d(t) + jF_q(t))e^{j\omega t} \tag{3}$$

Where H_d and H_q are respectively the real and imaginary part of the deflection, F_d and F_q are the real and imaginary part of the external force and ω is the excitation frequency which is also the pulsation of the resonator in this paper.

By deriving two times the Eq.2

$$\dot{\underline{\eta}} = [(\dot{H}_d + j\dot{H}_q) + j\omega(H_d + jH_q)]e^{j\omega t} \tag{4}$$

$$\ddot{\underline{\eta}} = [(\ddot{H}_d + j\ddot{H}_q) + 2j\omega(\dot{H}_d + j\dot{H}_q) - \omega^2(H_d + jH_q)]e^{j\omega t} \tag{5}$$

By replacing the Eq. (2) (3) (4) and (5) into (1) a system of two differential equation are obtained. The resulting equations can be expressed as a state space

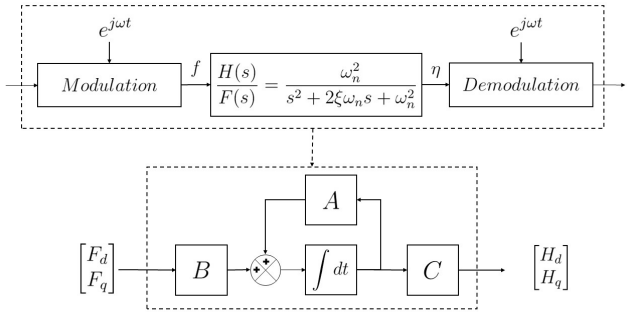

Figure 1: The equivalent model of a damped harmonic oscillator in a demodulated form

representation, and we have:

$$\begin{aligned} \dot{x} &= Ax + Bu \\ \begin{bmatrix} \dot{H}_d \\ \dot{H}_q \\ \ddot{H}_d \\ \ddot{H}_q \end{bmatrix} &= \begin{bmatrix} 0 & 0 & 1 & 0 \\ 0 & 0 & 0 & 1 \\ \omega^2 - \omega_n^2 & 2\xi\omega\omega_n & -2\xi\omega_n & 2\omega \\ -2\xi\omega\omega_n & \omega^2 - \omega_n^2 & -2\omega & -2\xi\omega_n \end{bmatrix} \begin{bmatrix} H_d \\ H_q \\ \dot{H}_d \\ \dot{H}_q \end{bmatrix} + \begin{bmatrix} 0 & 0 \\ 0 & 0 \\ \omega_n^2 & 0 \\ 0 & \omega_n^2 \end{bmatrix} \begin{bmatrix} F_d \\ F_q \end{bmatrix} \\ y = Cx &= \begin{bmatrix} 1 & 0 & 0 & 0 \\ 0 & 1 & 0 & 0 \end{bmatrix} \begin{bmatrix} H_d \\ H_q \\ \dot{H}_d \\ \dot{H}_q \end{bmatrix} \end{aligned} \tag{6}$$

Where the output is $y = [H_d, H_q]^T$.

Hence, by applying the transformation of the Eq. (2) and Eq. (3), we obtain an equivalent model of the harmonic oscillator into the demodulated state space, which dynamic depends on the difference between the resonance frequency ω_n and the operating frequency ω. The equivalent scheme of this representation is shown in the Fig.1. The Fig.2 shows an example of demodulated signals.

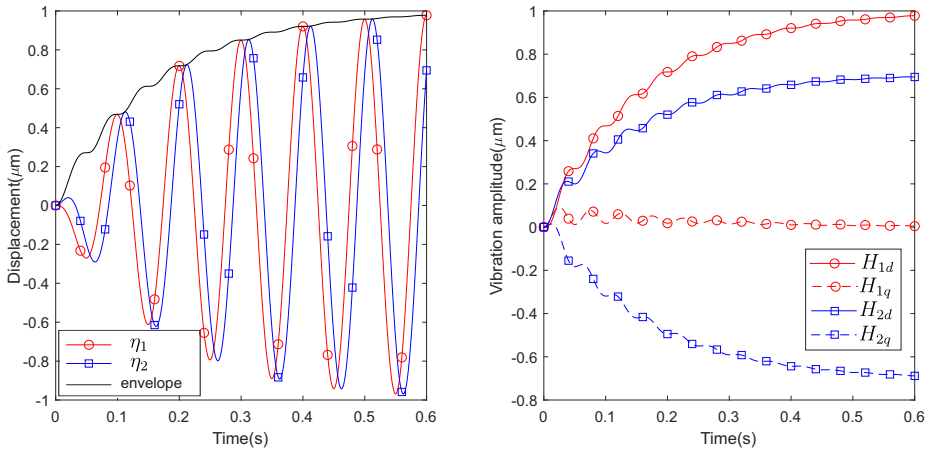

Figure 2: Example of a Demodulated signals : (left) example of two vibration signals with the same envelope and with different phases, and their (right) real and imaginary parts when demodulated.

2.2. Normalized Model

For sake of generality, the state space representation of the Eq. (6) is written in a normalized form that depends only on the damping ξ and the relative frequency $\Omega = \frac{\omega}{\omega_n}$. For that purpose, we define a new time base $\theta = \omega_n t$, and the state variables are revised into:

$$H_{nd} = H_d \qquad H'_{nd} = \frac{dH_{nd}}{d\theta} = \frac{\dot{H}_d}{\omega_n} \qquad H''_{nd} = \frac{d^2 H_{nd}}{d\theta^2} = \frac{\ddot{H}_d}{\omega_n^2} \tag{7}$$

$$H_{nq} = H_q \qquad H'_{nq} = \frac{dH_{nq}}{d\theta} = \frac{\dot{H}_q}{\omega_n} \qquad H''_{nq} = \frac{d^2 H_{nq}}{d\theta^2} = \frac{\ddot{H}_q}{\omega_n^2} \tag{8}$$

Introducing these new variables into the Eq. (6), yields:

$$\dot{x}_n = A_n x_n + B_n u_n$$

$$\begin{bmatrix} H'_{nd} \\ H'_{nq} \\ H''_{nd} \\ H''_{nq} \end{bmatrix} = \begin{bmatrix} 0 & 0 & 1 & 0 \\ 0 & 0 & 0 & 1 \\ \Omega^2 - 1 & 2\xi\Omega & -2\xi & 2\Omega \\ -2\xi\Omega & \Omega^2 - 1 & -2\Omega & -2\xi \end{bmatrix} \begin{bmatrix} H_{nd} \\ H_{nq} \\ H'_{nd} \\ H'_{nq} \end{bmatrix} + \begin{bmatrix} 0 & 0 \\ 0 & 0 \\ 1 & 0 \\ 0 & 1 \end{bmatrix} \begin{bmatrix} F_d \\ F_q \end{bmatrix} \tag{9}$$

To analyze the dynamic of the system in its demodulated space, we first calculate the characteristic polynomial of the plant $P(\lambda_n) = det(\lambda_n I - A_n)$

which gives:

$$P(\lambda_n) = \lambda_n^4 + 4\xi\lambda_n^3 + (4\xi^2 + 2\Omega^2 + 2)\lambda_n^2 + 4\xi(1-\Omega^2)\lambda_n + \Omega^2(\Omega^2 + 4\xi^2 - 2) + 1 \quad (10)$$

The eigen values of this plant do not have general form. However, for the specific case of a low damped oscillator ($\xi < 1$), they can be approximated by:

$$\begin{aligned} \lambda_{n(1,2)} &= -\xi \pm j(\Omega + \sqrt{1-\xi^2}) \\ \lambda_{n(3,4)} &= -\xi \pm j(\Omega - \sqrt{1-\xi^2}) \end{aligned} \quad (11)$$

Hence, compared with the system in its natural state space, the poles in the demodulated form resembles the poles of a second order system to which are added the demodulation term $\pm j\omega$ (or $\pm j\Omega$ for normalised model)[9]. By operating the resonator close to its resonant frequency ($\Omega = 1$), 2 poles of the system get closer to the real axis, as depicted in Fig. 3.

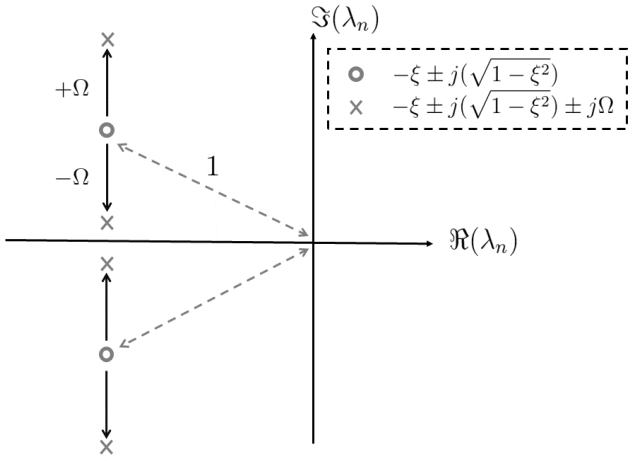

Figure 3: Eigenvalues of a second order system, in a normalized time base, before and after demodulation (respectively circles and crosses).

This normalized representation of the system in the demodulated state space allows us to consider the general design of the controllers, as presented in the next section of this paper.

3. General design of the controllers

3.1. State feedback to MIMO-PID

In this work, we present a method to control the resonator's oscillation using MIMO-PID state feedback controller in the demodulated state space, and the parameters of this controller are calculated using an LQR approach.

Let's consider the augmented state space representation which yields:

$$\dot{\hat{x}}_n = \hat{A}_n \hat{x}_n + \hat{B}_n u_n$$

$$\begin{bmatrix} H_{nd} \\ H_{nq} \\ H'_{nd} \\ H'_{nq} \\ H''_{nd} \\ H''_{nq} \end{bmatrix} = \begin{bmatrix} 0 & 0 & 1 & 0 & 0 & 0 \\ 0 & 0 & 0 & 1 & 0 & 0 \\ 0 & 0 & & & & \\ 0 & 0 & & & & \\ 0 & 0 & & A_n & & \\ 0 & 0 & & & & \end{bmatrix} \begin{bmatrix} \int H_{nd} \\ \int H_{nq} \\ H_{nd} \\ H_{nq} \\ H'_{nd} \\ H'_{nd} \end{bmatrix} + \begin{bmatrix} 0 & 0 \\ 0 & 0 \\ & \\ B_n & \\ & \end{bmatrix} \begin{bmatrix} F_d \\ F_q \end{bmatrix} \tag{12}$$

Therefore, the MIMO-PID controller consists then to write the input $u_n = [F_d, F_q]^t$ as:

$$\begin{aligned} u_n = K_n \tilde{x}_n = K_n(\hat{x}_{nref} - \hat{x}_n) &= \begin{bmatrix} K_{ni} & K_{np} & K_{nd} \end{bmatrix} \tilde{x}_n \\ &= \begin{bmatrix} k_{ni1} & k_{ni2} \\ k_{ni3} & k_{ni4} \end{bmatrix} \begin{bmatrix} \int \tilde{H}_{nd} \\ \int \tilde{H}_{nq} \end{bmatrix} + \begin{bmatrix} k_{np1} & k_{np2} \\ k_{np3} & k_{np4} \end{bmatrix} \begin{bmatrix} \tilde{H}_{nd} \\ \tilde{H}_{nq} \end{bmatrix} + \\ &\quad \begin{bmatrix} k_{nd1} & k_{nd2} \\ k_{nd3} & k_{nd4} \end{bmatrix} \begin{bmatrix} \tilde{H}'_{nd} \\ \tilde{H}'_{nq} \end{bmatrix} \end{aligned} \tag{13}$$

Where $\tilde{x}_n = [\int \tilde{H}_{nd}, \int \tilde{H}_{nq}, \tilde{H}_{nd}, \tilde{H}_{nq}, \tilde{H}'_{nd}, \tilde{H}'_{nq}]$ and where $\tilde{H}_{nd} = H_{nd} - H_{dref}$ and $\tilde{H}_{nq} = H_{nq} - H_{qref}$. The design of this controller needs then 12 parameters to be chosen to give an optimized behaviour of the system. In the following section, we apply the LQR method to optimally determine the value of these parameters.

3.2. PID Controller tuning via LQR approach

To get an optimal K_n feedback matrix, one of the most popular methods is to use an LQR approach, as it allows to reduce the transient of tracking

error (response time/overshoot) while minimizing the control effort [17]. The LQR approach consists in finding a state feedback (13) minimizing the following criteria J:

$$J = \int_0^\infty (\hat{x}_n^T Q \hat{x}_n + u_n^T R u_n) dt \tag{14}$$

Where Q is semi positive definite ($Q \geq 0$) and R positive definite ($R > 0$). These matrix can be tuned to get the desired performance while respecting the actuators maximum effort. It can be shown that a solution to this optimization problem, is to give K_n the following expression [17]:

$$K_n = R^{-1} \hat{B}_n^T P \tag{15}$$

where P is the solution of the algebraic Riccati equation ($P \geq 0$)

$$P\hat{A}_n + \hat{A}_n^T P + Q - P\hat{B}_n R^{-1} \hat{B}_n^T P = 0 \tag{16}$$

Tuning the closed loop system is then achieved through the matrices R and Q. However, in this system, since H_{nd} and H_{nq} are two component of the same signal, there is no reason to favour the imaginary part over the real part (and vice-versa), and the matrices R and Q will be chosen as follows:

$$\begin{aligned} Q &= diag[q_i, q_i, q_p, q_p, 0, 0] \\ R &= diag[1, 1] \end{aligned} \tag{17}$$

Where q_i and q_p are the weighting gains associated respectively with the integrals ($\int \tilde{H}_{nd} d\theta$, $\int \tilde{H}_{nq} d\theta$) and proportionals ($\tilde{H}_{nd}$, $\tilde{H}_{nq}$); the weighting gains associated with the derivatives are left equal to zero in order to reduce the amplification of measurement noise. It is a known effect due to the amplification of the signals at high frequencies, where the noise level is higher [19, p.615]. In vibration amplitude control, the objective is to achieve an exponentially convergent envelop with a given rising time, from 10% to 90% of the steady state value. To quantify the effect of the weighting gains, we define the following speed and shape criteria:

- $lg(\alpha) = lg(\frac{t_r}{t_{rc}})$ is the decimal logarithm of the ratio between the rising time in open-loop (t_r) and in closed-loop (t_{rc}), this indicator is defined

as the acceleration factor. Since the study assumes that the operating frequency is at resonance $\Omega = 1$, the dominant poles ($\lambda_{n(3,4)}$) are then purely real, according to Eq.11. Hence, t_r is approximately $t_r \simeq 2.2/(\xi\omega_n)$. We can also express α as $lg(\alpha) = lg(\frac{\xi_c}{\xi})$, where ξ_c is the closed-loop damping.

- $lg(\gamma) = lg(\frac{t_{rc}}{2.2\tau_c})$, where τ_c is defined as the settling time from 0% to 63.8% of the steady state value. This value was chosen because it corresponds to the time constant of a first order system.

An acceptable closed loop dynamic is reached if the desired rise time in closed loop is obtained. Moreover the time response should be exponentially convergent which is achieved if the closed loop rise time ($10\% - 90\%$) equals 2.2 times the closed loop time constant ($0\% - 63.8\%$). Thus, the following condition $lg(\gamma) = 0$ should be respected. In practice, the response is considered to be exponentially convergent for $|lg(\gamma)| < 0.02$.

To illustrate the effect of q_i and q_p, the fig.4(a-c) shows the criteria $lg(\alpha)$ and $lg(\gamma)$ as a function of the weighting gains q_i and q_p, for $\xi = 10^{-4}$ and $\Omega = 1$. The fig.4 (a) shows that in order to have a given α there is several couple q_i and q_p that lead to the same result. However, considering time response depicted in the Fig.4 (c), one can observe that the exponential convergence is not guaranteed in the region A and C of the Fig.4 (b). Hence, considering that this exponential convergence is obtained if $|lg(\gamma)| < 0.02$, we remove from 4-a the zones A and C depicted on the 4-b where this condition is not fulfilled, giving rise to fig.4-d. This can be ensured by constraining q_i and q_p along a line as depicted in black on the same figure. On this line, we write $lg(q_i) = a \times lg(q_p) + b$ with $a = 1$ and $b = -8$.

As shown in the Fig.4-(d:i), the same procedure is performed for $\xi \in \left[10^{-7}, 10^{-2}\right]$ and for each plot the values of a and of the coordinates $[lg(q_{p0}), lg(q_{i0})]$ for which $lg(\alpha) = 0$ (i.e $t_r = t_{rc}$) are taken; the results are given in the table 1.

From the Tab 1, several approximations can be made. First, a is supposed

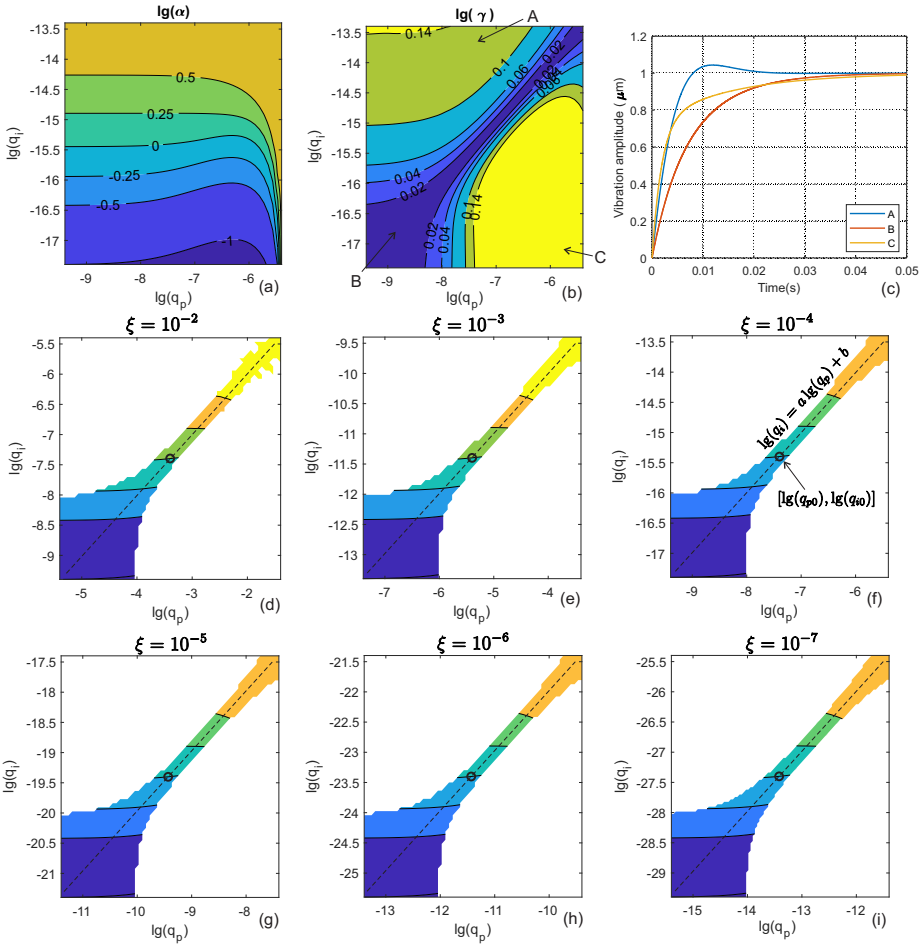

Figure 4: Closed loop performances as a function of the weighting parameters (q_p and q_i) : (a) relation between the acceleration factor $lg(\alpha)$ and the weighting parameters for $\xi = 10^{-4}$, (b) relation between the indicator $lg(\gamma)$ and the weighting parameters for $\xi = 10^{-4}$, (c) examples of closed-loop time responses when the weighting parameters are chosen in zone A,B and C and for $\xi = 10^{-4}$, (d-i) relation between the acceleration factor $lg(\alpha)$ and the weighting parameters by eliminating all the zone where $|lg(\gamma)| > 0.02$ for different value of ξ

$\lg(\xi)$	-7	-6	-5	-4	-3	-2
a	1.0000	1.0000	1.0000	0.9999	1.0000	0.9913
b	-13.9950	-12.0000	-10.0000	-7.9894	-6.0000	-4.0292
$\lg(q_{p0})$	-13.3939	-11.4177	-9.3933	-7.3933	-5.4177	-3.3708
$\lg(q_{i0})$	-27.3889	-23.7177	-19.3933	-15.3820	-11.4177	-7.3708

Table 1: Polynomial's parameters (a,b) of the relation $lg(q_i) = a \times lg(q_p) + b$ and coordinates $[lg(q_{p0}), lg(q_{i0})]$ where $lg(\alpha) = 0$

to be invariant and equal to 1, leading to:

$$\lg\left(\frac{q_i}{q_{i0}}\right) = \lg\left(\frac{q_p}{q_{p0}}\right) \tag{18}$$

Second, $\lg(q_{p0})$ and $\lg(q_{i0})$ can be approximated by a linear interpolation and we write:

$$\begin{aligned} \lg(q_{p0}) &= 2 \times \lg(\xi) + 0.6021 \approx 2 \times \lg(\xi) + \lg(4) = \lg(4\xi^2) \\ \lg(q_{i0}) &= 4 \times \lg(\xi) + 0.6021 \approx 4 \times \lg(\xi) + \lg(4) = \lg(4\xi^4) \end{aligned} \tag{19}$$

At this point, the methodology gives the weighting parameters such that a system with damping ξ will have the same dynamic in closed-loop as in open-loop. So, the next step is to establish a relation between $\lg(\alpha)$, $\lg(q_p)$, $\lg(q_i)$, while imposing the Eq.(18). By this way, the weighting parameters can be calculated for any system damping $\xi \in [1 \times 10^{-7}, 1 \times 10^{-2}]$ and for any desired dynamic α. The relation between $\delta = \lg(q_p/q_{p0})$ and $\lg(\alpha)$ for different values of ξ is shown in the Tab 2 . From the values in this table, it can be observed that for a given δ, $\lg(\alpha)$ is almost invariant (less than 0.1% for $\xi \in [1 \times 10^{-7}, 1 \times 10^{-2}]$), while, for a given ξ, δ varies almost linearly. Therefore, a linear interpolation can be applied as follows $\lg(\alpha) = a_\alpha \times \lg(q_p/q_{p0}) + \ b_\alpha$.

Tab 3 gathers the coefficient of the linear regression within a considered range for $\xi \in [1 \times 10^{-7}, 1 \times 10^{-2}]$ and $\delta \in [-2, 2]$. It can be observed that 1) a_α is constant, 2) b_α is small compared to the practical range of $\lg(\alpha)$, 3) the norm of the residuals $||e||$ decreases with ξ and are always smaller than 2.04×10^{-2}. Since b_α is small enough, the relation between $\lg(\alpha)$ and $\lg(q_p/q_{p0})$ is further

δ \ ξ	10^{-7}	10^{-6}	10^{-5}	10^{-4}	10^{-3}	10^{-2}
-2.0	-1.0000	-1.0000	-1.0000	-1.0000	-1.0001	-0.9998
-1.5	-0.7500	-0.7500	-0.7500	-0.7500	-0.7501	-0.7498
-1.0	-0.5000	-0.5000	-0.5000	-0.5000	-0.5001	-0.4997
-0.5	-0.2500	-0.2500	-0.2500	-0.2500	-0.2501	-0.2496
0.0	0.0000	0.0000	0.0000	0.0000	-0.0002	0.0004
0.5	0.2500	0.2500	0.2500	0.2500	0.2498	0.2479
1.0	0.5000	0.5000	0.5000	0.5001	0.5003	0.4978
1.5	0.7500	0.7500	0.7501	0.7500	0.7497	0.7460
2.0	1.0000	1.0000	1.0000	1.0001	0.9990	1.0000

Table 2: Relation between $\delta = \lg(q_p/q_{p0})$ and $\lg(\alpha)$ for different values of $\xi \in [10^{-7}, 10^{-2}]$

$\lg(\xi)$	-7	-6	-5	-4	-3	-2
a_α	0.5000	0.5000	0.5000	0.5000	0.5000	0.5000
b_α	$1.34e^{-4}$	$-1.23e^{-4}$	$4.24e^{-5}$	$4.36e^{-5}$	$4.30e^{-5}$	$4.30e^{-5}$
$\|\|e\|\|$	$2.04e^{-2}$	$2.8e^{-3}$	$2.07e^{-4}$	$2.56e^{-5}$	$4.33e^{-6}$	$1.16e^{-6}$

Table 3: Polynomial's parameters (a_α, b_α) of the relation $\lg(\alpha) = a_\alpha \times \lg(q_p/q_{p0}) + b_\alpha$ for different values of $\xi \in [10^{-7}, 10^{-2}]$, and the norm of the residuals $||e||$

simplified as:

$$\lg(\alpha) = a_\alpha \times \lg\left(\frac{q_p}{q_{p0}}\right) = \frac{1}{2} \times \lg\left(\frac{q_p}{q_{p0}}\right) \tag{20}$$

Considering a range of $\alpha\xi \leq 10^{-1}$, the Eq. (20) gives α with an accuracy of at least 99.5%. By replacing the Eq.(19) and the Eq.(18) into the Eq.(20), we can write an empirical formula of the weighting gains in function of the desired dynamic

$$\begin{aligned} \lg(q_p) &= 2 \times \lg(\alpha) + \lg(4\xi^2) \\ \lg(q_i) &= 2 \times \lg(\alpha) + \lg(4\xi^4) \end{aligned} \tag{21}$$

After simplifying the equations we get

$$\begin{aligned} q_p &= (2\alpha\xi)^2 = (2\xi_c)^2 \\ q_i &= (2\alpha\xi^2)^2 = (2\xi_c\xi)^2 \end{aligned} \tag{22}$$

At this point, the weighting coefficients q_p and q_i can be expressed directly from the system parameter ξ and the design parameter α which sets the closed-loop dynamic. It is now possible to use them in order to define systematically the Q and R matrices of Eq. (17) and proceed to solve the Riccati equation for the normalized system yielding the state feedback matrix K_n of the Eq.(13).

The normalized controller is calculated by

$$\begin{bmatrix} F_d \\ F_q \end{bmatrix} = \begin{bmatrix} k_{ni1} & k_{ni2} \\ k_{ni3} & k_{ni4} \end{bmatrix} \begin{bmatrix} \int \tilde{H}_{nd} \\ \int \tilde{H}_{nq} \end{bmatrix} + \begin{bmatrix} k_{np1} & k_{np2} \\ k_{np3} & k_{np4} \end{bmatrix} \begin{bmatrix} \tilde{H}_{nd} \\ \tilde{H}_{nq} \end{bmatrix} + \begin{bmatrix} k_{nd1} & k_{nd2} \\ k_{nd3} & k_{nd4} \end{bmatrix} \begin{bmatrix} \tilde{H}'_{nd} \\ \tilde{H}'_{nq} \end{bmatrix} \tag{23}$$

The last step is to define the actual gains. For a specific plant with the resonance frequency ω_n, they are deduced from the obtained generalized controller by applying the variable change $\tilde{H}_{nd} = \tilde{H}_d = H_{dref} - H_d$, $\tilde{H}_{nq} = \tilde{H}_q = H_{qref} - H_q$, $\int \tilde{H}_{nd} d\theta = \omega_n \int \tilde{H}_d dt$, $\int \tilde{H}_{nq} d\theta = \omega_n \int \tilde{H}_q dt$, $\tilde{H}'_{nd} = \frac{d\tilde{H}_d}{d\theta} = \frac{\dot{\tilde{H}}_d}{\omega_n}$ and $\tilde{H}'_{nq} = \frac{d\tilde{H}_q}{d\theta} = \frac{\dot{\tilde{H}}_q}{\omega_n}$. Finally, the implemented controller is written

$$\begin{bmatrix} F_d \\ F_q \end{bmatrix} = \omega_n \begin{bmatrix} k_{ni1} & k_{ni2} \\ k_{ni3} & k_{ni4} \end{bmatrix} \begin{bmatrix} \int \tilde{H}_d \\ \int \tilde{H}_q \end{bmatrix} + \begin{bmatrix} k_{np1} & k_{np2} \\ k_{np3} & k_{np4} \end{bmatrix} \begin{bmatrix} \tilde{H}_d \\ \tilde{H}_q \end{bmatrix} + \frac{1}{\omega_n} \begin{bmatrix} k_{nd1} & k_{nd2} \\ k_{nd3} & k_{nd4} \end{bmatrix} \begin{bmatrix} \dot{\tilde{H}}_d \\ \dot{\tilde{H}}_q \end{bmatrix} \tag{24}$$

The resulting closed loop control scheme is shown in the Fig.5

4. Experimental set-up and protocol

4.1. Experimental set-up

In this experimental validation, the strategy is used to control a resonant plate actuated by piezoelectric ceramics (see Fig.6-a) used in a haptic tactile

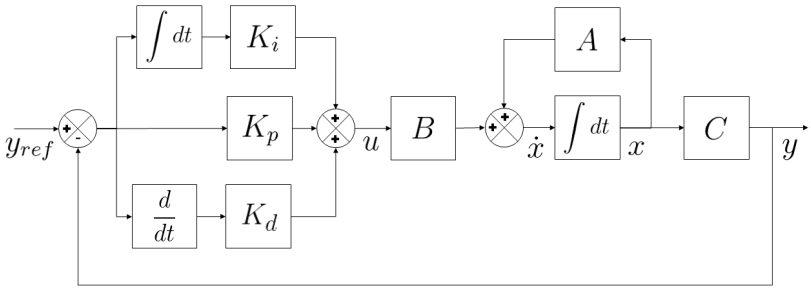

Figure 5: Closed loop control scheme

feedback experiment.

The developed set-up includes STM32F4 (FEZ CERB 40 GHI Electronics LLC) to implement the demodulation, the controller and the modulation. The signals are linearly amplified using a high voltage operational amplifier OPA 445 (Texas instrument). To achieve the voltages required to operate the ceramics (up to 200 V peak), the output voltage of the amplifier is further amplified by a resonant circuit realized by introducing an inductance in series that interact with the blocked capacitance of the piezoelectric ceramics. The inductance is designed to ensure that the electric resonant frequency matches approximately the mechanical resonance. The actual tactile feedback device consists in a $18 \times 119 \times 2\text{mm}^3$ aluminum plate to exploit the first plate bending mode at 24 860 Hz. The identified mode shape, identified using a laser vibrometer (Polytec OFV 505), is depicted in Fig.6-b). Below the plate, four piezoelectric ceramics ($16 \times 4 \times 0.5\text{mm}^3$) are glued, three of them are used to actuate the plate. The remaining is connected to one of the STM32 ADC inputs and is used as a vibration sensor.

4.2. Control scheme

The control implemented (shown in the Fig.7) in this experiment is similar to the one described in [10] which involves two asynchronous process. First, Direct Digital Synthesis (DDS), with frequency 1 MHz (T_s =1 µs), generates the voltage reference that is then amplified to supply the actuators. Since for

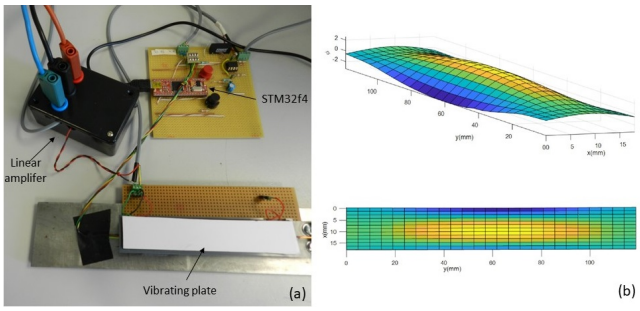

Figure 6: (a) The vibrating plate and it's control unit, (b) identified mode shape $\phi_k(x, y)$ of the 1x1 bending mode

piezoelectric ceramics the generated force is proportional to the voltage v, we can write in Eq. (1) $f = gv$ and

$$\underline{v} = (V_d + jV_q)e^{j\omega t} \tag{25}$$

The voltage is generated using the real part of eq.25

$$v\left(t_k\right) = V_d \cos\left(\omega t_k\right) - V_q \sin\left(\omega t_k\right) \tag{26}$$

Where $t_k = kT_s$ and k is the sample number. Similarly to [10] the discrete value of H_d and H_q are calculated as follows

$$H_d(t_k) = \sum_{n=0}^{N_s-1} \eta(t_{k-n}) \cos\left(\omega t_{k-n}\right) \tag{27}$$

$$H_q(t_k) = \sum_{n=0}^{N_s-1} \eta(t_{k-n}) \sin\left(\omega t_{k-n}\right) \tag{28}$$

where N_s is the number of samples over a period of the oscillation $T = \frac{2\pi}{\omega}$. A slower process is implemented at a rate of 10 kHz. In closed-loop, it calculates and updates the voltages components V_d, V_q. In open loop, it is used for dynamic identification and tests, as discussed in the following section.

4.3. Parameters identification

In some circumstances, the parameters can vary due to environmental variations such as temperature or modified boundary conditions during tests. In

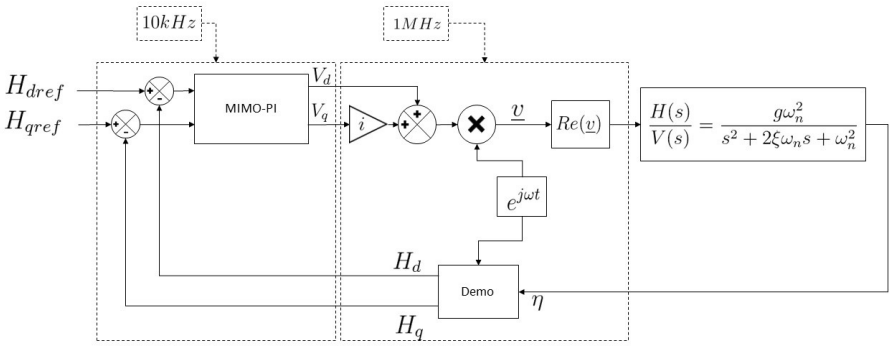

Figure 7: Feedback control scheme

order to identify the dynamic parameters g, ξ and ω_n in Eq. (6) an identification procedure is performed. It consists in a frequency sweep with bandwidth of $2\Delta\omega$ around an a priori resonance frequency $\hat{\omega}_n$ such that $\omega = \hat{\omega}_n \pm \Delta\omega$, with a constant input voltage. For each value of ω the steady state values of H_d and H_q are measured. It is also necessary to take into account the non-linear behaviour of the structure. So, the identification procedure is performed for different levels of the input voltage.

Once this acquisition performed, the damping factor ξ is calculated using the extrema of the real part H_d. Let ω_1 and ω_2 be the angular frequency where H_d is maximum and minimum (cf Fig. 8) respectively, then, one can verify that:

$$\xi = \frac{1}{2}\frac{1 - \frac{\omega_1^2}{\omega_2^2}}{1 + \frac{\omega_1^2}{\omega_2^2}} \tag{29}$$

Since the argument of $\underline{H} = H_d + jH_q$ are close to $\frac{-\pi}{4}$ and $\frac{-3\pi}{4}$ respectively for ω_1 and ω_2 if the damping ξ is small, these points are simple to identify in practice. With the same assumption on the damping, one can consider that the resonance frequency ω_n corresponds to the maximum gain frequency. Thus, the static gain g is deduced from:

$$g = -2 \times \xi \times \Im\left[\frac{H(j\omega_n)}{V(j\omega_n)}\right] \tag{30}$$

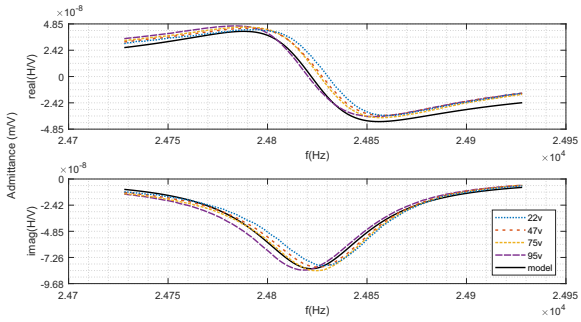

Figure 8: Frequency response of the plate with different input voltage and frequency response of the nominal model

To handle the structural non-linearity which is responsible for slight variation of the resonance with the vibration amplitude, for each measurement series with a given voltage, a corresponding model's parameters set is identified. According to this procedure, the obtained nominal parameters are g =2.6834 $\times 10^{-10}\,\mathrm{m\,V^{-1}}$; ξ =1.4 $\times 10^{-3}$; ω_n =1.5596 $\times 10^{5}\,\mathrm{rad\,s^{-1}}$. The Fig.8 shows the real and imaginary part of the frequency response for different input voltages, and the response of the nominal model is shown in dashed-lines.

4.4. Controller implementation

The method discussed so far yields a PID, even if the weighting associated with the derivative action is kept nul in Eq.(17) . The derivative action can be a problem as it tends to amplify measurement noise. The case of continuous and discrete implementation of the control are examined in Fig. 9. In this figure, the closed loop poles are normalized by Ω in order to compare oscillators with different dynamics. Concerning the discrete case, the sampling time used in the computation of the poles is chosen large enough to respect the Nyquist frequency with regards to the dynamics $\alpha\xi\Omega$.

Considering the continuous case, if the derivative actions resulting from the LQR procedure are omitted, the high frequency poles at 2Ω are shifted toward the right as the value of α is increased rapidly resulting in an unstable pole pair. By contrast, including the derivative action induce the opposite behaviour, hence

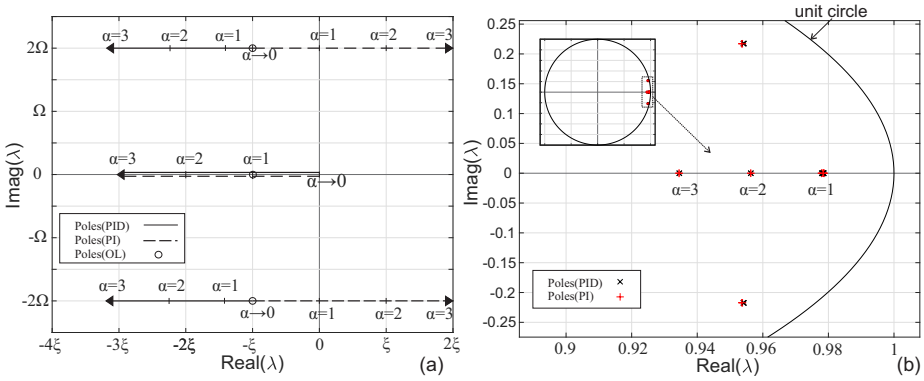

Figure 9: Poles location of the closed loop for a continuous (left) and discrete (right) PI and PID controllers (resp. dashed and plain lines). In the continuous case, the derivative action is required to prevent destabilization as the high frequency poles at 2Ω contrarily to the discrete case.

no instability is possible.

This contrasts with discrete case, where the high frequency poles remain mostly unchanged with regards to the choice of α for the PI and PID controllers. Hence, in this work, the derivative action is omitted in the following tests.

4.5. Results

In order to validate the control approach presented in this paper, a comparison between different desired dynamics (α=[0.25, 0.5, 1.0, 1.5, 2.0, 2.5, 3.0, 3.5, 4.0]) and experimental obtained dynamics is presented. The value of α are used to calculate the MIMO-PID gains by using the approach developed in the previous section. Since the implemented controller is discretized, we consider that a MIMO-PI is sufficient in order to have the same performances. Indeed, the Fig.9-b shows the closed-loop discrete poles when using a MIMO-PID or a MIMO-PI controller for different α values. The figure show that the poles and zeros are quasi-identical when using a PID or a PI discrete controller.

The controller gains are then implemented in the DSP. In each case, the closed loop step response of the resonant plate is recorded, her the reference vector H_{dref} =0.5 µm,H_{qref} =0 µm. The Fig. 10 shows some examples of tests

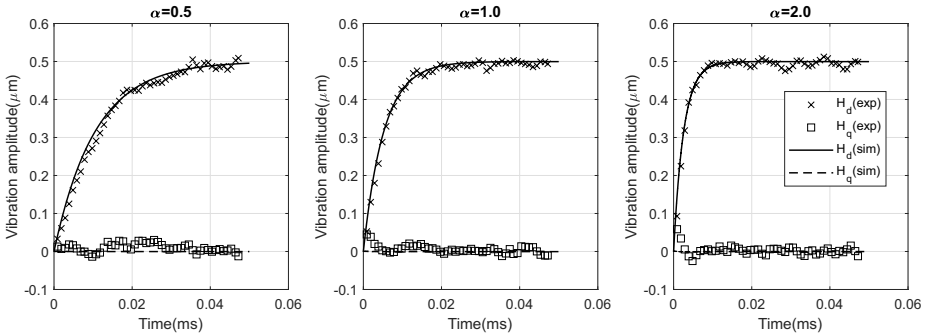

Figure 10: Step response for $\alpha = (0.5, 1.0, 2.0)$

where the time response is slower, equal or faster than the natural time response of the plate. On the same figure, the theoretical responses are superimposed, showing a good agreement between prediction and measurement. Oscillations can also be observed, which are more important for higher α. They are caused by the spillover effect due to neighbour modes. Since the vibrations signal are demodulated, the oscillation frequency corresponds to the difference between the controlled mode and the neighbour mode. A large choice of α induces a larger closed-loop bandwidth and thus increases the spillover effect, which is not considered in the model (6).

To further assess the theory discussed above, the Fig. 11 depicts the logarithm of the time response to a reference for various α. The tendency is linear as expected. Based this figure, the slope α_{exp} is identified and compared to the theoretical values α on table 4. However, it can be noted that for low values of α, the discrepancy between theory and measurement can be large. Actually, this is due to the fact the gain implemented to slow down the transient are small. As a consequence, the voltage applied is small, and results in a coarse output voltage once converted by the digital to analog conversion. Hence, the seemingly constant output at start-up and steady-state that can be observed for $\alpha = 0.25$, and results in a rough linear approximation. For high values of α, however, the good agreement proves that the simplifying hypothesis proposed in the theory are verified and it demonstrates the validity of the method.

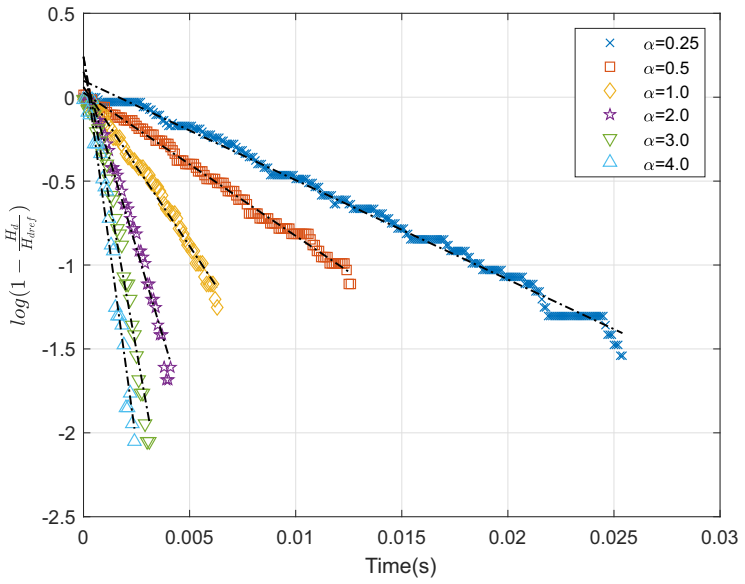

Figure 11: Logarithm of the time response to a reference ($\log(1-\frac{H_d}{H_{dref}})$) for various α, the slope of the fitted lines corresponds to the closed-loop time constant $1/(\xi_c\omega_n)$

α	0.25	0.5	1	1.5	2	2.5	3	3.5	4
α_{exp}	0.314	0.453	1.01	1.58	1.99	2.40	3.95	3.56	3.93
$err(\%)$	25.6	9.4	7.0	5.3	0.7	3.8	1.5	1.8	1.8

Table 4: Experimental acceleration ratios α_{exp} and the error (in percent)

5. Conclusion

A method to design systematically the controller for a resonator in a rotating frame was discussed. First, the model was presented in a state space form, and the design of the controller is based on a LQR optimal controller. The novelty of the proposed design is to relate directly the weight matrices Q and R to relevant performances indexes that guarantee a given time response and an envelop of the vibration during the transient. This reveals a simple relationship linking the α index, that governs the time response, to the weighting factors implemented in the Q and R matrices. The experimental results demonstrate a good agreement between the theory and the measurements despite some technological limitation such as the digital/analog conversion. A second issue is the spillover effect that limit the practical choice for α.

Acknowledgement

The authors would like to thank the CNRS/IRCICA-USR 3380 research center, which hosted the research.

References

[1] R. Gabai, D. Ilssar, R. Shaham, N. Cohen, I. Bucher, A rotational traveling wave based levitation device - modelling, design, and control, Sensors and Actuators A: Physical 255 (2017) 34–45. doi:10.1016/j.sna.2016.12.016.

[2] W. B. Messaoud, F. Giraud, B. Lemaire-Semail, M. Amberg, M. Bueno, Amplitude Control of an Ultrasonic Vibration for a Tactile Stimulator, IEEE/ASME Transactions on Mechatronics 21 (3) (2016) 1692–1701. doi:10.1109/TMECH.2016.2535300.

[3] S. Davis, I. Bucher, Automatic vibration mode selection and excitation; combining modal filtering with autoresonance, Mechanical Systems and

Signal Processing 101 (2018) 140–155. doi:10.1016/j.ymssp.2017.08.009.

[4] X. Liu, A. I. Colli-Menchi, J. Gilbert, D. A. Friedrichs, K. Malang, E. Sánchez-Sinencio, An Automatic Resonance Tracking Scheme With Maximum Power Transfer for Piezoelectric Transducers, IEEE Transactions on Industrial Electronics 62 (11) (2015) 7136–7145. doi:10.1109/TIE.2015.2436874.

[5] B. Borovic, A. Liu, D. Popa, H. Cai, F. Lewis, Open-loop versus closed-loop control of mems devices: choices and issues, Journal of Micromechanics and Microengineering 15 (10) (2005) 1917.

[6] V. Babitsky, V. Astashev, A. Kalashnikov, Autoresonant control of nonlinear mode in ultrasonic transducer for machining applications, Ultrasonics 42 (1) (2004) 29 – 35, proceedings of Ultrasonics International 2003. doi:https://doi.org/10.1016/j.ultras.2004.01.004.

[7] T.-C. Chen, C.-H. Yu, C.-J. Chen, M.-C. Tsai, Neuro-fuzzy speed control of traveling-wave type ultrasonic motor drive using frequency and phase modulation, ISA Transactions 47 (3) (2008) 325 – 338. doi:https://doi.org/10.1016/j.isatra.2008.04.001.

[8] A. Bazaei, S. R. Moheimani, Synthesis of modulated-demodulated control systems, Automatica 50 (7) (2014) 1816–1824. doi:10.1016/j.automatica.2014.05.015.

[9] K. S. Karvinen, S. O. R. Moheimani, Modulated-Demodulated Q Control of an Atomic Force Microscope Microcantilever, IFAC Proceedings Volumes 46 (5) (2013) 399–405. doi:10.3182/20130410-3-CN-2034.00093.

[10] S. Ghenna, F. Giraud, C. Giraud-Audine, M. Amberg, Vector Control Of Piezoelectric Transducers and Ultrasonic Actuators, IEEE Transactions on Industrial Electronics PP (99) (2017) 1–1. doi:10.1109/TIE.2017.2784350.

[11] K. M. A. Kadhar, S. Baskar, S. M. J. Amali, Diversity Controlled Self Adaptive Differential Evolution based design of non-fragile multivariable PI controller, Engineering Applications of Artificial Intelligence 46 (2015) 209–222. doi:10.1016/j.engappai.2015.09.015.

[12] J.-B. He, Q.-G. Wang, T.-H. Lee, PI/PID controller tuning via LQR approach, Chemical Engineering Science 55 (13) (2000) 2429–2439. doi:10.1016/S0009-2509(99)00512-6.

[13] S. Mukhopadhyay, P.I.D. equivalent of optimal regulator, Electronics Letters 14 (25) (1978) 821–822. doi:10.1049/el:19780555.

[14] K. H. Estévez-Sánchez, A. Sampieri-Croda, M. A. García-Alvarado, I. I. Ruiz-López, Design of multiloop PI controllers based on quadratic optimal approach, ISA Transactions 70 (2017) 338–347. doi:10.1016/j.isatra.2017.07.011.

[15] S. Das, I. Pan, K. Halder, S. Das, A. Gupta, LQR based improved discrete PID controller design via optimum selection of weighting matrices using fractional order integral performance index, Applied Mathematical Modelling 37 (6) (2013) 4253–4268. doi:10.1016/j.apm.2012.09.022.

[16] S. Das, I. Pan, S. Das, Multi-objective LQR with optimum weight selection to design FOPID controllers for delayed fractional order processes, ISA Transactions 58 (2015) 35–49. doi:10.1016/j.isatra.2015.06.002.

[17] A. Preumont, Vibration Control of Active Structures: An Introduction, 4th Edition, Solid Mechanics and Its Applications, Springer International Publishing, 2018.

[18] L. Meirovitch, Fundamentals of Vibrations, McGraw-Hill, 2001.

[19] K. Ogata, Modern Control Engineering, 4th Edition, Prentice Hall PTR, Upper Saddle River, NJ, USA, 2001.